doi:10.1038/nature09681

1. IRAC Photometry

Spitzer IRAC fluxes were measured from a combination of programs 20070 (COSMOS) , 40801, 50310 and 61043 (SEDS) in the COSMOS field. The data for program 61043 were obtained during the Spitzer warm mission and only the data obtained in January 2010 were used for this paper. The average exposure time at the position of the proto-cluster is 6.3 hours per pixel.

The data reduction procedure closely follows that used for the COSMOS data (program 20070)[29]. We began our reduction using the corrected basic calibrated data (cBCD) provided by the Spitzer Science Center. The cBCDs were background matched using the contributed afrl_bcd_overlap IDL procedure, and then combined into a mosaic using the MOPEX software package. Cosmic rays, asteroids, and other transient artefacts were removed using the MOPEX temporal and box outlier modules. The images were combined using a drizzle interpolation with a PIXFRAC of 0.65 and an exposure time weighted co-addition. The resulting image has a 1 sigma, background limited, point source sensitivity of 38 nJy and 44 nJy in 3.6μm and 4.5μm respectively for the region around the proto-cluster.

Fluxes were measured by fitting an empirically measured point spread function (PSF) at the source position. Compact sources within 5 arc-minutes of the proto-cluster were used to construct the PSF model. For un-confused sources the PSF fit fluxes agreed well with 3.8" diameter aperture photometry measurements corrected to total flux via a statistical aperture correction. The new IRAC fluxes for the sources are given in Supplementary Table 1.

2. 2mm Observations of COSMOS AzTEC-3

The Goddard-IRAM Superconducting 2-Millimeter Observer (GISMO) is a bolometer camera optimized for 2-millimeter observations at the IRAM 30m telescope. GISMO uses a closed packed 128 element transition edge sensor (TES) detector array with an instantaneous field of view of 2'x4'. The observations of AzTEC-3 were obtained on April 12, 2010 with 100 minutes of integration. Flux calibrations were obtained to 18% accuracy with observations of Mars and pointing was verified by frequent observations of the nearby quasar J0948+003. The data were reduced and calibrated using the CRUSH-2 data reduction package.

We detect a source with 3.1σ significance based on the 18" beam-smoothed flux maps and the noise maps within the expected positional error of AzTEC-3. Including the statistical, calibration, and positional errors the detection of AzTEC-3 has a 99% statistical probability. We estimate the 2mm flux to be 3.7±1.4 mJy including uncertainty from the flux calibration. We note the 2mm flux is not corrected for possible flux boosting[14] since this correction factor requires knowledge of the 2mm number counts and these are not well measured.

3. Selecting Cluster Members

One of the great strengths of the COSMOS data are the extremely accurate ($dz/(1+z)<0.01$) photometric redshfits at $z<1.5$[30]. However, the techniques used to construct the photometric redshifts suffer from catastrophic failures when applied to high redshift and extreme sources such as those in our proto-cluster. Supplementary Figure 1 shows a comparison of the spectroscopic[31,32] and photometric[30] redshifts for objects brighter than $i<26$ including a sample of 168 spectroscopic redshifts at $z>3$ in the COSMOS field. We found >40% of luminous $z>4$ objects are placed at $z<2$ by the photometric redshift method, including the extreme starburst presented here. This is primarily due to photometric contamination from foreground sources. When low-levels of flux are spuriously found in the photometry blue-ward of the 912Å break the photometric redshifts find a low-redshift solution. However, we also found cases at fainter flux levels where a low redshift solution was preferred because the photometric limits could not rule it out.

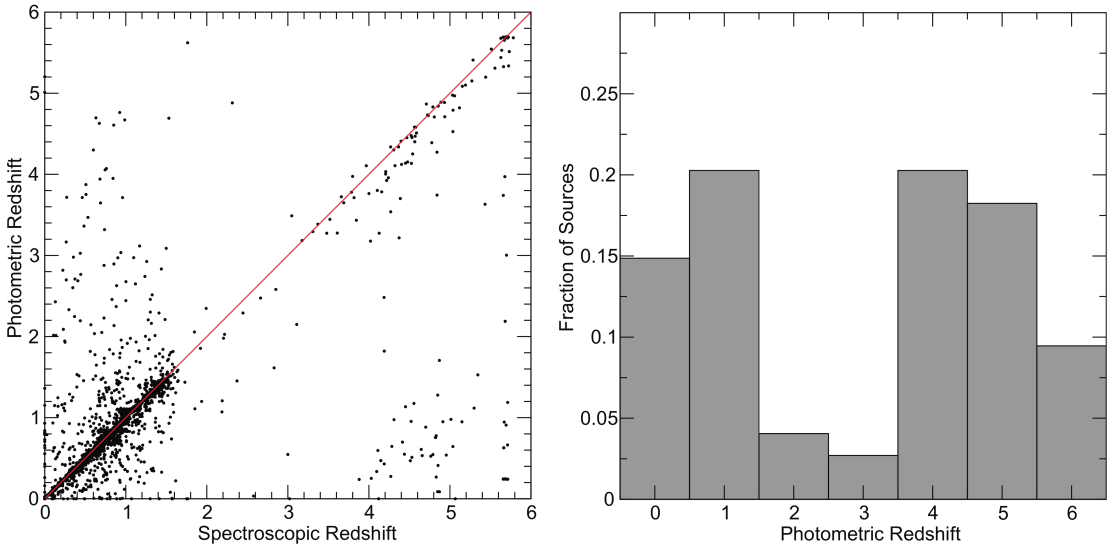

Supplementary Figure 1: A comparison of the photometric[30] and spectroscopic[31,32] redshifts for faint objects in the COSMOS field is shown on the left. In addition to the previously published results, this plot includes 167 objects at $z>3$ and >2200 objects fainter than $I>22.5$. In the right panel the photometric redshift distribution for 148 objects with spectroscopic redshifts at $z>4$ is shown. Note that 39.2% of objects are placed at $z<3$.

Rather than suffer the limitations of the photometric redshifts we chose to use a colour selection to identify potential proto-cluster members. The colour selection focuses on the region of the spectral energy distribution with maximum information. Furthermore, by limiting the number of filters used we avoid smoothing the images to the resolution of the worst seeing images and thereby maximizing the signal-to-noise of the photometry while minimizing contaminating light from foreground sources.

Photometry was measured using a procedure similar to that of the general COSMOS catalog[21]. However, rather than matching the point spread function (PSF) to 3” diameter apertures, the PSF homogenized images and a 1” and 2” diameter aperture

was used. A statistical aperture correction was then applied to each band to bring the aperture magnitudes into average agreement with the 3" PSF matched aperture photometry from the COSMOS catalogue[21].

A simulated photometric catalogue was used to define a z~5.3 selection criteria. The simulation assumed the measured evolution of the UV luminosity function between 0<z<3 and no evolution at z>3. The distribution of galaxy types and obscuration was matched to the comprehensive spectroscopic sample in GOODS-N. However, the selection function is broadly insensitive to the exact assumptions made in the model, with decreased ages, decreased dust obscuration, and evolution at z>3 all narrowing the redshift distribution.

Using this simulation, we defined our colour criteria as no detection in a 1" diameter aperture at >3σ significance in the u, B, g, and V bands along with colours of r-i>1 and IA738-i > 0.3. This selects a combination of z=5.36±0.2 galaxies, galactic M, L, T stars and faint (low mass) z~0.85 galaxies with old stellar populations and/or large obscuration.

Stars are easily removed because of their very red z-J colours but blue J-H colours. Low mass galaxies are removed using the spectral bump at 1.6μm if they are sufficiently bright in the J,H,K and IRAC bands. However, for objects fainter than H>23.5 (i~25.5) (40% of our sample) we relied on the IRAC colours alone.

The uncertainty in the selection method has little impact on the conclusions. The objects with confirmed redshifts contain 65% of the proto-cluster mass, still within the range expected for a proto-cluster. Furthermore, the density of spectroscopically confirmed sources is significantly higher than that expected. Excluding objects without firm J,H,K detections only reduces the mass by 21% since these fainter objects tend to be the least massive.

4. Estimating the Magnitude and Significance of the Cluster

The significance of this cluster can be estimated from observational data[33,34] and from cosmological simulations[7]. Using our intermediate band colour selection to find galaxies at z=5.36±0.2 we find 8 objects in 1 square arc minute and 11 objects within a 2 Mpc (0.93 arc minute) radius of COSMOS AzTEC-3 brighter than I<26 (L_* at z=5.3)[19]. These objects also meet the V and r dropout Lyman-Break criteria, but fall on the high-redshift end of these selections, so we consider V, r, and I band dropouts as comparison samples.

A conservative estimate of the expected surface density can be derived using the Great Observatories Origins Deep Survey (GOODS) data[19]. In these data a surface density of 0.75+/-0.04 galaxies per square arc minute brighter than z_{850}<26.0 is found in the combined V-band and I-band dropout samples. These samples cover a redshift range of 4.5<z<6.5, a factor of five more volume than our selection. Furthermore, objects are brighter in the z_{850} filter than the I band, so the surface density is an over-estimate for an I band selected sample. However, even with this conservative estimate the region around COSMOS AzTEC-3 is over-dense by a factor of 11 in the 1 square arc minute region, and a factor of 5 within the 2 Mpc radius.

A better estimate of the significance can be obtained from the 4 square degree Canada-France-Hawaii Legacy Deep Survey (CFHT-LS Deep) data[20]. These data find a surface density of 0.352+/-0.006 r-dropout (4.5<z<5.2) galaxies per square arc minute brighter than z'<26 and a 2-point correlation function described by a clustering length (r_o) of 5.53 h^{-1} Mpc and a power-law index of γ=2.13. Using the correlation function we estimate a variance of 1.06 galaxies in a 2 Mpc radius circle over the redshift interval probed by the r-band dropouts[20]. Using the mean density and variance, the cluster is 11.5 times over-dense and has a significance of 9.5σ.

The significance was also estimated using a simulated 2 square degree galaxy catalogue based on the Millennium simulation[35]. From the possible semi-analytics in this simulation we chose the WMAP 3yr cosmology, Galaxy formation Model C, and Dust Model 2 which most closely match the observed properties of z>3 galaxies. Galaxies were selected form the simulated catalogue to match the redshift distribution of the observed samples[20], and a magnitude limit of I<26.1 was adopted to match the observed object surface densities[20]. For the r-dropout selection function and a 2 Mpc radius cell we find a mean galaxy density of 0.94 and a variance of 1.14 galaxies per cell, meaning the observed cluster is an 11.7 times over-density with a significance of 8.8σ.

Alternatively, using the intermediate band selection function of z=5.36±0.2 we find a mean galaxy density of 0.14 and a variance of 0.39 galaxies per cell, a factor of 78.6 over-density, formally significant at 27.8σ. However, if we scale the r-band dropout surface density to the volume of the intermediate band selection and assume the same clustering properties, we find the significance is only 14.4σ.

Finally, if we consider only the three spectroscopically confirmed galaxies, a redshift interval of 5.3±0.005, and the measured r-band dropout clustering and space density we expect 0.024 galaxies in the 2Mpc cell with a variance of 0.19, implying a factor of 125 over-density significant at 16.7σ.

In summary, we find this region is over-dense by a factor of >11 at the >9σ level, with the spectroscopic sub-sample suggesting an even higher significance.

5. Estimating Stellar Masses

To determine stellar masses models[24] were fit to the data red-ward of the Lyman-alpha forest break at rest frame 1216Å. These data included the IA827, NB816, z+, J, H, and Ks band photometry from the COSMOS catalog[21], and the IRAC 3.6μm and IRAC 4.5μm band photometry presented here. In the case of the extreme starburst the IRAC 5.8μm and 8.0μm detections[29] were also used. The properties of the proto-cluster members within 2 Mpc of the starburst are given in Supplementary Table 1. The optical ID numbers and positions are those from the COSMOS catalog[21], while the 3.6μm and 4.5μm fluxes are derived from the new Spitzer data described in supplementary section 1. The ages, dust obscuration (Av), and Masses are determined from our model fitting and are accurate to 3 Myr, 0.2 magnitudes and 0.3 dex respectively, however these errors are highly correlated and subject to systematic uncertainties in the underlying stellar population models.

Supplementary Table 1: Model fitting results

Optical ID	RA J2000	DEC J2000	Age (Myr)	Av (Mag)	Stellar Mass (log10[$M_\odot$])	3.6μm flux (nJy)	4.5μm flux (nJy)
1445777	150.09148	2.602377	3	1.4	9.1	336±46	256±64
1445840	150.0937	2.600853	3	0.25	7.8	<38	<44
1446425	150.0839	2.598316	2.5	0.25	7.9	<38	<44
1446767	150.08328	2.595851	4.5	1.5	9.3	344±46	431±64
1447523	150.08573	2.589246	3	0.85	8.8	348±52	145±66
1447524*	150.08958	2.575765	8	0.5	9.5	1372±48	2039±66
1447526	150.08654	2.586426	10	0.4	9.4	563±46	717±46
1447531*+	150.08625	2.58933	10	0.8	10.0	1419±48	2159±68
1448834	150.08309	2.588966	9	1.0	9.2	169±46	407±64
1449472	150.07305	2.582372	9	0.6	9.3	372±46	708±64

*Spectroscopically confirmed
+Starburst

6. Estimating The Infrared Luminosity of COSMOS AzTEC-3

The infrared luminosity was estimated empirically from the mm, radio limits, and CO line fluxes. The 1.1mm continuum measurement yields Far Infrared (60-120μm) luminosities (L_{FIR}) between 0.9-2 x10^{13} $L_\odot$ assuming sub-mm slopes of 3.5 and 3 respectively. The actual spectral slope is constrained to be >3 at long wavelengths by the 870μm, 1.1mm and 2mm measurements[14,15] along with the 2.7, 3.2, and 8.2mm continuum limits obtained with the CO measurements[8], suggesting the source is cold and of lower intrinsic luminosity.

Evidence for cold dust is also supported by the flux ratios of the 870μm to 3.3mm data. The 870μm fluxes yield L_{FIR} values that are 30% lower than those obtained with the 1.1mm flux alone and the 1.1mm flux yields a L_{FIR} 80% lower than the 2mm flux alone. The 870μm data are near the dust emission peak at this redshift, and hence are likely to under-estimate L_{FIR} if the dust temperature is low. Furthermore, the 1.1-3.3mm L_{FIR} estimates are only consistent if the sub-mm spectral slope is >3.5.

Using the L_{FIR} to radio correlation[16,36] with q=2.35 and a spectral slope of -0.8, we estimate L_{FIR} <1.5 x10^{13} $L_\odot$. Instead, using the L'CO- L_{FIR} relation[37] we find L_{FIR}=1.3 x10^{13} $L_\odot$.

Fitting models to the 24μm through radio photometry yields similar results given in Supplementary Table 2 and shown in Supplementary Figure 2. We note that the scatter in model estimates of L_{IR} is much greater than the estimates of L_{FIR}. This reflects differing assumptions in the models since the data does not constrain rest frame wavelengths shorter than 140μm.

Combing these estimates we find $L_{FIR}=1.7\pm0.8\times10^{13}\ L_{\odot}$.

Supplementary Table 2: Infrared model fitting results

Template	Model Name	χ^2	L_{FIR} (60-120μm) ($L_{\odot}$)	L_{IR}(8-1000μm) ($L_{\odot}$)
Chary & Elbaz[38]	$L_{IR}=10^{12.15}$	2.4	2.3×10^{13}	6.8×10^{13}
Dale & Helou[39]	1.1875	2.2	3.2×10^{13}	1.1×10^{14}
Lagache Hot[40]	$L_{IR}=10^{9}$	11.5	1.6×10^{13}	3.4×10^{13}
Lagache Cold[40]	$L_{IR}=10^{9.2}$	6.9	6.9×10^{12}	2.2×10^{13}

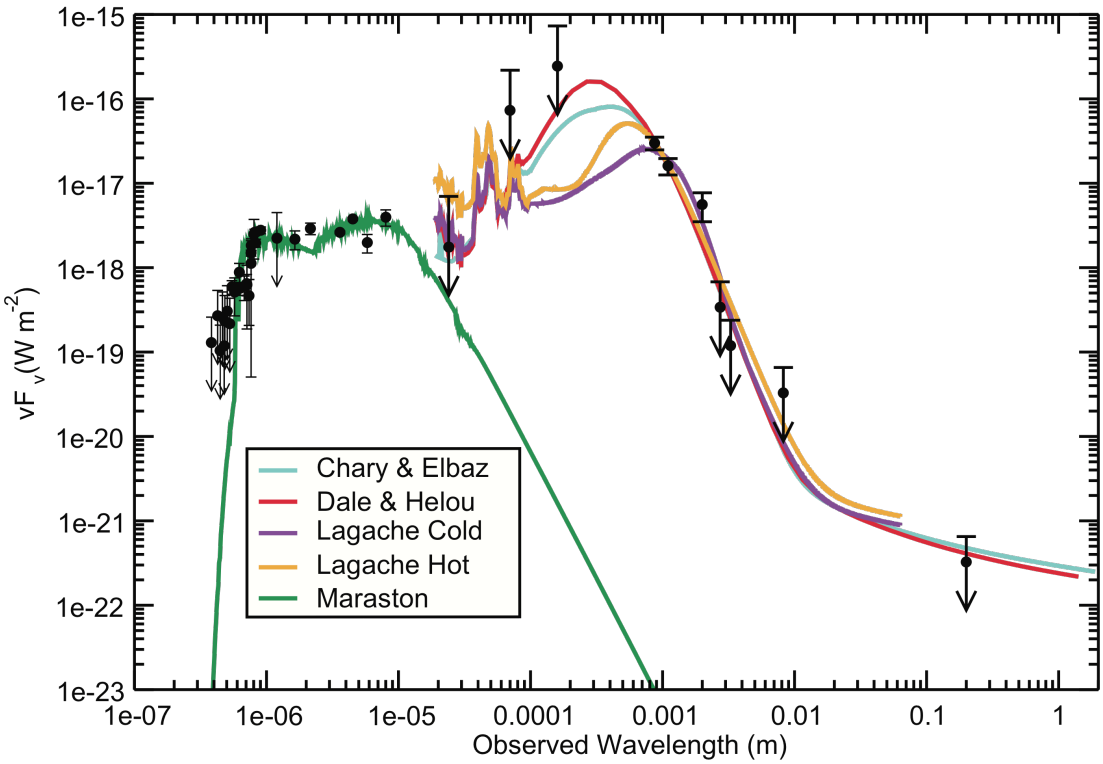

Supplementary Figure 2: The spectral energy distribution of COSMOS AzTEC-3 is shown along with model fits[24,38,39,40]. Error bars are 1σ including standard measurement error and systematic flux calibration error. The optical, near and mid-infrared, and radio data are taken from the COSMOS survey[16,21,29], with newly acquired warm IRAC data used at 3.6 and 4.5μm. The 0.87 and 1.1mm fluxes are taken from the sub-mm imaging survey[14,15], wile the 2mm data point presented here was acquired with the GISMO camera on the IRAM 30m telescope. The 2.7, 3.3, and 8.2mm flux limits are from the CO 6-5, 5-4, and 2-1 measurements[8]. The best-fit stellar mass is $1.0\pm0.3 \times 10^{10}$ solar masses with A_v=0.8 and an age of 10Myr. The best fit Far-Infrared (60-120μm) luminosity ranges from $0.9\text{-}3.2 \times 10^{13}$ solar luminosities depending on the model assumptions. However, the 3mm upper limits, the radio flux limit, and the CO luminosity favor lower luminosities.

Supplementary References

29. Sanders, D.B *et al*. S-COSMOS: The Spitzer Legacy Survey of the Hubble 5Space Telescope ACS 2 deg2 COSMOS Field I: Survey Strategy and First Analysis. *Astrophys. J. Supp*., **172**, 86-98 (2007).

30. Ilbert, O. *et al*. COSMOS Photometric Redshifts with 30-bands for 2-deg^2. *Astrophys. J*., **690**, 1236-1249 (2009).

31. Lilly, S.J. *et al*. The zCOSMOS 10k-Bright Spectroscopic Sample. *Astrophys. J. Supp*., **184**, 218-229 (2009)

32. Trump, J. R. *et al*. Magellan Spectroscopy of AGN Candidates in the COSMOS Field. *Astrophys. J. Supp*., **172**, 383-394 (2007)

33. Somerville, R.S. *et al*. Cosmic Variance in the Great Observatories Origins Deep Survey. *Astrophys. J. Lett*., **600**, 171-174 (2004).

34. Robertson, B.E. Estimating Luminosity Function Constraints from High-Redshift Galaxy Surveys. *Astrophys. J*., **713**, 1266-1281 (2010).

35. Wang J., *et al*. The dependence of galaxy formation on cosmological parameters: can we distinguish between the WMAP1 and WMAP3 parameter sets? *Mon. Not. R. astro. Soc*., **384**, 1301-1315 (2008).

36. Carilli, C. & Yun, M. The Scatter in the Relationship between Redshift and the Radio-to-Submillimeter Spectral Index. *Astrophys. J*., **530**, 618-624 (2000)

37. Riechers, D. *et al*. CO(1-0) in z >~ 4 Quasar Host Galaxies: No Evidence for Extended Molecular Gas Reservoirs. *Astrophys. J*., **650**, 604-613 (2006)

38. Chary, R. & Elbaz, D. Interpreting the Cosmic Infrared Background: Constraints on the Evolution of the Dust-enshrouded Star Formation Rate. *Astrophys. J*., **556**, 562-581 (2001)

39. Dale, D. & Helou, G. The Infrared Spectral Energy Distribution of Normal Star-forming Galaxies: Calibration at Far-Infrared and Submillimeter Wavelengths. *Astrophys. J*., **576**, 159-168 (2002)

40. Lagache, G., Dole, H., & Puget, J.-L. Modelling infrared galaxy evolution using a phenomenological approach. *Mon. Not. R. astro. Soc*., **338**, 555-571 (2003).